

1 **Neuronal modeling of magnetoencephalography responses in auditory cortex to**
2 **auditory and visual stimuli**

3 *Kaisu Lankinen^{1,2}, Jyrki Ahveninen^{1,2}, Mainak Jas^{1,2}, Tommi Raij^{1,2}, Seppo P. Ahlfors^{1,2}*

4 *¹ Athinoula A. Martinos Center for Biomedical Imaging, Massachusetts General Hospital,*
5 *Charlestown, MA 02129*

6 *² Department of Radiology, Harvard Medical School, Boston, MA 02115*

7

8

9 Corresponding author: Kaisu Lankinen, klankinen@mgh.harvard.edu

10 Abbreviated title: Modeling cross-sensory MEG responses

11 Number of pages: 38

12 Number of figures: 7

13 Number of tables: 1

14 Number of words for abstract: 230

15 Number of words for introduction: 571

16 Number of words for discussion: 1517

17

18 Conflict of interest: The authors declare no competing financial interests.

19

20 Acknowledgments: Supported by R01DC016765, R01DC016915, R01DC017991,
21 P41EB030006, P41EB015896. We thank Dr. Stephanie Jones for useful discussions.

22 **ABSTRACT**

23 Previous studies have demonstrated that auditory cortex activity can be influenced by cross-
24 sensory visual inputs. Intracortical recordings in non-human primates (NHP) have suggested a
25 bottom-up feedforward (FF) type laminar profile for auditory evoked but top-down feedback (FB)
26 type for cross-sensory visual evoked activity in the auditory cortex. To test whether this principle
27 applies also to humans, we analyzed magnetoencephalography (MEG) responses from eight
28 human subjects (six females) evoked by simple auditory or visual stimuli. In the estimated MEG
29 source waveforms for auditory cortex region of interest, auditory evoked responses showed peaks
30 at 37 and 90 ms and cross-sensory visual responses at 125 ms. The inputs to the auditory cortex
31 were then modeled through FF and FB type connections targeting different cortical layers using
32 the Human Neocortical Neurosolver (HNN), which consists of a neocortical circuit model linking
33 the cellular- and circuit-level mechanisms to MEG. The HNN models suggested that the measured
34 auditory response could be explained by an FF input followed by an FB input, and the cross-
35 sensory visual response by an FB input. Thus, the combined MEG and HNN results support the
36 hypothesis that cross-sensory visual input in the auditory cortex is of FB type. The results also
37 illustrate how the dynamic patterns of the estimated MEG/EEG source activity can provide
38 information about the characteristics of the input into a cortical area in terms of the hierarchical
39 organization among areas.

40

41 **SIGNIFICANCE STATEMENT**

42 Laminar intracortical profiles of activity characterize feedforward- and feedback-type influences in
43 the inputs to a cortical area. By combining magnetoencephalography (MEG) and biophysical
44 computational neural modeling, we obtained evidence of cross-sensory visual evoked activity in
45 human auditory cortex being of feedback type. The finding is consistent with previous intracortical
46 recordings in non-human primates. The results illustrate how patterns of MEG source activity can
47 be interpreted in the context of the hierarchical organization among cortical areas.

48

49 INTRODUCTION

50 Activity in sensory cortices is influenced by feedforward (FF) and feedback (FB) connections
51 between cortical layers and brain regions, following a hierarchical organization (Rockland and
52 Pandya, 1979; Felleman and Van Essen, 1991; Zeki, 2018). In the auditory cortex of non-human
53 primates (NHPs), the laminar profile of early auditory evoked responses has FF type
54 characteristics, whereas cross-sensory visual or somatosensory evoked activity are of FB type
55 (for reviews see, e.g., Foxe and Schroeder, 2005; Schroeder and Foxe, 2005; Ghazanfar and
56 Schroeder, 2006; Kayser and Logothetis, 2007). Human magneto- and electroencephalography
57 (MEG/EEG) studies have revealed that cross-sensory activations and multisensory interactions
58 can occur in low-order sensory areas very early, within a few tens of milliseconds from the
59 stimulus onset (Giard and Peronnet, 1999; Foxe et al., 2000; Molholm et al., 2002; Teder-Sälejärvi
60 et al., 2002; Molholm et al., 2004; Lakatos et al., 2007; Talsma et al., 2007; Raij et al., 2010). In
61 line with evidence from studies in other cognitive domains (Polimeni et al., 2010; Muckli et al.,
62 2015; Kok et al., 2016; Fracasso et al., 2018; Klein et al., 2018; Finn et al., 2019; Lawrence et al.,
63 2019a; Norris and Polimeni, 2019), recent high-field fMRI studies have provided evidence of FF-
64 and FB-like intracortical depth profiles in auditory cortex BOLD signals (De Martino et al., 2015;
65 Ahveninen et al., 2016; Moerel et al., 2018; Wu et al., 2018; Moerel et al., 2019; Gau et al., 2020;
66 Chai et al., 2021; Lankinen et al., 2022). However, detailed neurophysiological analysis or
67 computational modeling of such effects has not been done in humans.

68 Previous studies have suggested that early components of evoked responses are related to
69 FF processes, whereas later components reflect FB influences in activity evoked by auditory (Inui
70 et al., 2006; Kohl et al., 2022), visual (Aine et al., 2003; Inui and Kakigi, 2006), and somatosensory
71 (Cauller and Kulics, 1991; Inui et al., 2004; Jones et al., 2007) stimuli.

72 Biophysically realistic computational models have been used to investigate laminar
73 connections and cellular and circuit level processes of the neurons in detail, and they can also be

74 used to simulate MEG/EEG signals (Jones et al., 2007; Neymotin et al., 2020). The Human
75 Neocortical Neurosolver (HNN) (Neymotin et al., 2020) provides a cortical column model with FF-
76 and FB-type inputs targeting different layers. With HNN, the cellular and network contributions to
77 MEG/EEG signals from a source-localized region of interest can be modeled and compared to
78 the measured signals. Previously, HNN has been used to interpret mechanisms of sensory
79 evoked responses and oscillations in healthy and clinical populations (Jones et al., 2007; Jones
80 et al., 2009; Ziegler et al., 2010; Lee and Jones, 2013; Khan et al., 2015; Sherman et al., 2016;
81 Pinotsis et al., 2017; Sliva et al., 2018; Bonaiuto et al., 2021; Kohl et al., 2022; Law et al., 2022).
82 Kohl et al. (2022) showed that auditory responses in the auditory cortex could be modeled by
83 activating the neocortical circuit through a layer-specific sequence of FF-FB-FF inputs, similar to
84 a prior simulation of somatosensory evoked responses (Jones et al., 2007).

85 In the present study, we investigated auditory vs. cross-sensory visual evoked responses in
86 the auditory cortex by comparing the measured MEG responses with simulated source waveforms
87 from a computational model (HNN). We hypothesized that the auditory evoked responses
88 observed with MEG can be explained by a sequence of FF and FB influences, whereas FB-type
89 input is adequate to explain the cross-sensory visual evoked response.

90

91

92 MATERIAL AND METHODS

93 *Subjects*

94 Eight healthy right-handed subjects participated (six females, age 22–30 years). All subjects gave
95 written informed consent, and the study protocol was approved by the Massachusetts General
96 Hospital institutional review board and followed the guidelines of the Declaration of Helsinki.

97 *Stimuli and task*

98 The subjects were presented with *Noise/Checkerboard* and *Letter* stimuli in separate runs while
99 MEG was recorded. Data for the *Noise/Checkerboard* stimuli were used in our earlier publication
100 (Raij et al., 2010). Here we re-analyzed data from the *Noise/Checkerboard* experiment, together
101 with the previously unpublished data from the *Letter* experiment. Equiprobable 300-ms auditory,
102 visual, and audiovisual (simultaneous auditory and visual) stimuli were delivered in an event-
103 related design with pseudorandom order. The auditory *Noise* stimuli were white noise bursts (15
104 ms rise and decay) and the visual *Checkerboard* stimuli static checkerboard patterns (visual angle
105 $3.5^\circ \times 3.5^\circ$ and contrast 100%, with a peripheral fixation crosshair). The *Letter* stimuli were spoken
106 and written letters of Roman alphabet ('A', 'B', 'C', etc.). The subjects' task was to respond to rare
107 (10%) auditory, visual, or audiovisual target stimuli with the right index finger movement as quickly
108 as possible. In the *Noise/Checkerboard* experiment, the target stimulus was a tone pip, a
109 checkerboard with a gray diamond pattern in the middle, or a combination of the two. In the *Letter*
110 task, the target stimulus was the letter 'K', spoken and/or written. Data were recorded in three
111 runs with different stimulus onset asynchrony (SOA, mean 1.5, 3.1, or 6.1 s, all jittered at 1.15 s).
112 There were 375 stimuli per category (auditory, visual, and audiovisual): 150 in the short, 125 in
113 the intermediate, and 100 in the long SOA runs. All subjects were presented with the same order
114 of tasks and stimuli. The auditory stimuli were presented with MEG-compatible headphones, with
115 the intensity adjusted to be as high as the subject could comfortably listen to. The visual stimuli

116 were projected onto a translucent screen. The stimuli were controlled using Presentation 9.20
117 (Neurobehavioral Systems Inc, Albany, CA, USA).

118 ***MEG and MRI acquisition and co-registration***

119 MEG was recorded with a 306-channel instrument with 204 planar gradiometer and 102
120 magnetometer sensors (VectorView; MEGIN, Finland) inside a magnetically shielded room
121 (Cohen et al., 2002). Simultaneous horizontal and vertical electro-oculograms (EOG) were also
122 recorded. All signals were bandpass-filtered to 0.03–200 Hz and sampled at 600 Hz.

123 Structural T1-weighted MRIs of the subjects were acquired with a 1.5 T Siemens Avanto
124 scanner (Siemens Medical Solutions, Erlangen, Germany) and a head coil using a standard
125 MPRAGE sequence. Cortical surfaces were reconstructed using the FreeSurfer software
126 (<http://www.surfer.nmr.mgh.harvard.edu>, (Fischl, 2012)).

127 Prior to the MEG recording, the locations of four small head position indicator coils attached to
128 the scalp and several additional scalp surface points were determined with respect to the fiducial
129 landmarks (nasion and two preauricular points) using a 3-D digitizer (Fastrak Polhemus, VT,
130 USA). For the MRI–MEG coordinate system alignment, the fiduciary points were first identified
131 from the structural MRIs, and then this initial co-registration was refined using an iterative closest-
132 point search algorithm for the scalp surface locations using the MNE Suite software (Gramfort et
133 al., 2014, <http://www.martinos.org/mne/>).

134 ***MEG preprocessing and source estimation***

135 The MEG data were analyzed using MNE-Python (Gramfort et al., 2013). After excluding channels
136 and time segments with excessive noise, independent component analysis (ICA) was used to
137 identify and remove artifacts related to eye blinks, eye movements, and cardiac activity. The
138 signals were then lowpass filtered at 40 Hz, and event-related responses were averaged
139 separately for the auditory and visual trials, combining the long, intermediate, and short SOA runs.

140 After exclusion of artifactual time segments an average of 369.9 (std 6.5) epochs per subject
141 remained in response to auditory, and 370.2 (std 5.1) to visual stimulation. In the present study
142 we did not analyze the audiovisual or target trials. The zero level in each channel was defined as
143 the mean signal over the 200-ms prestimulus baseline period.

144 Source activity was estimated at 4098 discrete locations per hemisphere on the cortical
145 surface, with an average separation of the source elements being about 4.9 mm. For the forward
146 solution, a single-compartment boundary element model was used. Forward solutions were first
147 computed separately for the three runs with different SOAs and then averaged (Uutela et al.,
148 2001). Minimum-norm estimates (MNE, (Hamalainen and Ilmoniemi, 1994)) for the cortical source
149 currents were calculated. Both the gradiometer and the magnetometer channels were included in
150 the source estimation. We used fixed source orientation normal to the cortical surface and depth
151 weighting 0.8 to reduce bias towards superficial currents. For region-of-interest (ROI) selection,
152 the MNE values were noise-normalized to obtain dynamic statistical parametric maps (dSPM;
153 Dale et al., 2000).

154 ***Regions-of-interest and source time courses***

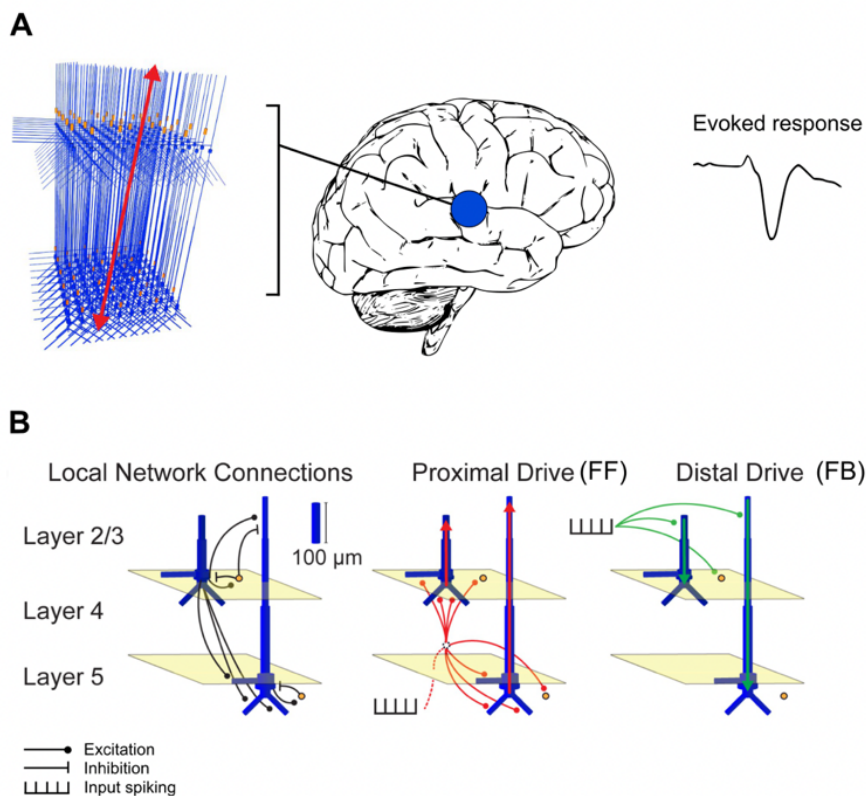
155 Auditory evoked potentials and magnetic fields typically have three main deflections: P50-N100-
156 P200 (or P50m-N100m-P200m for MEG), peaking approximately at 50, 100 and 180 ms,
157 respectively, after the auditory stimulus onset (Picton et al., 1974; Hari et al., 1980; Hämäläinen
158 et al., 1993; Jones et al., 2007; Ahlfors et al., 2015). The ROIs were determined based on the
159 auditory N100m response, because the SNR of the visual evoked response over the auditory
160 cortex was too low to reliably determine auditory cortex ROIs from the visual evoked data in the
161 presence of partially coinciding strong occipital visual cortex activity. We identified functional ROIs
162 for the auditory cortex in each hemisphere, separately for each subject, based on the N100m
163 peak of the auditory evoked response. First, anatomically defined regions were selected using
164 the Destrieux atlas parcellation from Freesurfer (Fischl et al., 2004; Destrieux et al., 2010):

165 Heschl's gyrus, Heschl's sulcus, and the lower part of planum temporale (masked with
166 supramarginal gyrus) were combined to cover the primary auditory areas. Then, from these
167 regions the source element with the largest negative deflection between 60–110 ms (except for
168 manually set 105 ms in one subject) in the dSPM source time course was identified. Using that
169 source element as a seed point, all source elements that had a magnitude of 30% or more of the
170 peak dSPM value and formed a continuous area around the seed point were selected. The
171 average number of selected elements across subjects, hemispheres and experiments for the
172 auditory cortex ROIs was 19 (standard deviation 8.7, range 3–38). The same procedure was used
173 to determine also additional control ROIs in the occipital cortex (V1, V2, and MT based on the
174 FreeSurfer atlas (Fischl et al., 2008). The source waveform for an ROI was defined as the sum of
175 the MNE time courses over those selected source elements. Note that the magnitude of the
176 response depended on the number of the vertices that were included in the ROI, and thus was
177 expected to give a smaller amplitude than would be found by the use of a single equivalent current
178 dipole to represent the auditory cortex activity (as used, e.g., by Kohl et al. (2022)). Although
179 equivalent current dipoles are in general well suited to describe auditory evoked responses, here
180 it was more convenient to use a distributed source model (MNE) for wide-spread visual evoked
181 response, to extract cross-sensory responses in the auditory cortex.

182 ***Neural modeling with Human Neocortical Neurosolver (HNN)***

183 Activity in the auditory cortex evoked by the auditory and visual stimuli was modeled using HNN
184 (<https://jonescompneurolab.github.io/hnn-core/>) (Neymotin et al., 2020). HNN is a software for
185 simulating neocortical circuits and linking cellular- and circuit-level physiology to the electrical
186 source currents measured by MEG and EEG. Thus, HNN provides a tool to develop and test
187 hypotheses on the neural origins of MEG/EEG signals. The neural currents contributing to the
188 MEG/EEG signals from a source region are modeled in terms of the local network dynamics driven
189 by layer-specific inputs (see **Fig. 1**). Simulated MEG/EEG source currents are represented as

190 current dipole waveforms calculated from the distribution of intracellular currents in the dendrites
191 of the pyramidal cells. MEG/EEG signals originate mostly from postsynaptic currents in cortical
192 pyramidal neurons (Hämäläinen et al., 1993; Okada et al., 1997), and the magnitude and direction
193 of the source current depends on the type of the synaptic input and its dendritic location (Allison
194 et al., 2002; Jones et al., 2007; Linden et al., 2010; Lopes da Silva, 2010; Ahlfors et al., 2015;
195 Ahlfors and Wreh, 2015), providing a link between the laminar distribution of synaptic inputs and
196 the MEG/EEG source waveforms.



197
198 **Figure 1.** Schematic illustration of the HNN model. (A) A network of neurons in a local cortical
199 area generates an evoked response. (B) Local network structure with pyramidal cells (blue) and
200 interneurons (orange). Excitatory and inhibitory coupling is indicated by a black circle and bar,
201 respectively. The network is activated by proximal (red) and distal (green) drives by input spike
202 trains. Modified from Neymotin et al. (2020).

203 In HNN, the model for a local cortical circuit has a layered structure with pyramidal neurons
204 whose somata are in the supragranular (layer 2/3) or infragranular (layer 5) layers and whose
205 dendrites span across the layers. The model also includes inhibitory interneurons. External input
206 to the circuit arrives through characteristic layer-specific FF and FB type connections. FF type
207 inputs consist of proximal drives to the basal dendrites of the pyramidal cells (assumed to arrive
208 via the middle cortical layer), whereas FB inputs are represented by distal drive to the apical
209 dendrites of the pyramidal cells. The model has 100 pyramidal neurons in each of layers 2/3 and
210 5; a scaling factor is used to match the simulated dipole to the magnitude of the recorded evoked
211 response. The parameters of the HNN model originate from known anatomical and physiological
212 cell properties, and the local connectivity within and between cortical layers is based on a large
213 body of literature from animal studies (Jones et al., 2007; Neymotin et al., 2020).

214 We used HNN to test the hypothesis that the differences in the MEG responses to auditory
215 and visual stimuli can be explained by a different sequence of FF and FB inputs to the auditory
216 cortex. This hypothesis is based on neurophysiological evidence from animal studies (Schroeder
217 and Foxe, 2002). Underlying mechanisms of auditory responses in humans have been previously
218 described using HNN (Kohl et al., 2022). Our specific hypothesis was that the auditory response
219 can be explained by an initial FF input followed by an FB input, but the visual response just by an
220 FB input.

221 We created two main HNN models for event-related activity in the auditory cortex: one for the
222 response to auditory stimuli and one for the response to visual stimuli. The grand average MEG
223 source waveforms (averaged across subjects, hemispheres, and experiments) were modeled
224 using HNN. As a starting point, we used the auditory cortex model by Kohl et al. (2022) for activity
225 in the right hemisphere evoked by auditory stimuli presented to the left ear. Because HNN has a
226 large number of user-defined parameters, we made the following assumptions to limit the
227 parameter space: a) Only the timing parameters of the FF/FB spike-train inputs (mean μ and

228 standard deviation σ of a Gaussian distribution) were adjusted, in addition to an overall scaling
229 factor for the simulated source waveforms; all the other parameters were kept unchanged. b)
230 These other, internal, model parameters were assumed to be the same for the responses to visual
231 and auditory stimuli. c) The simulations were limited to the time window of 0–150 ms for the
232 auditory and 0–170 ms for the visual response, in order to focus on the early part of the responses.
233 HNN model parameters were determined by minimizing the root mean square error (RMSE)
234 between the simulated and experimentally observed MEG source waveforms. To improve the
235 SNR of the experimental data, we averaged MEG source waveforms over subjects, hemispheres,
236 and the two experiments. The simulated HNN waveforms were smoothed in the default 30-ms
237 window (Hamming window convolution).

238 We first manually adjusted the start time of the FF/FB inputs and scaling of the response to
239 achieve a close initial fit to the MEG responses. An optimal scaling factor was determined by
240 minimizing the RMSE between the average of 10 simulation runs and the MEG waveform over
241 the specified time windows. Thereafter, we further tuned the model parameters using Bayesian
242 optimization implemented in scikit-optimize (Head, 2020)
243 (<http://doi.org/10.5281/zenodo.1207017>) for estimating μ (mean input spike timing) and σ
244 (temporal distribution of input spikes) for each model by minimizing the RMSE between the
245 simulated and the measured signal. We used “expected improvement” as the acquisition function.
246 The initial parameters were defined from the manual fit and the bounds for the search space were
247 (μ_{FF} : 20...50, μ_{FB} : 55...95, μ_{FF2} : 90...130, σ_{FF} : 1...5, σ_{FB} : 5...20, σ_{FF2} : 5...20).

248 As HNN has a large number of parameters, it is possible that even after optimizing our main
249 models, some other combination of parameter values could explain the waveforms equally well
250 or better. Therefore, we formed alternative models by varying the number and timing of the FF
251 and FB inputs. We focused on the comparison of FF + FB vs. FB models for explaining the early
252 part of the MEG activity evoked by auditory and visual stimuli.

253 **Statistical analyses**

254 To evaluate whether the magnitudes of the estimated MEG source waveforms (averaged
255 across tasks and hemispheres) were significantly different from zero, we used *t*-tests with a
256 threshold $p < 0.05$ in each of the 150 time points in the 0–250 ms window. The *p*-values were
257 Bonferroni adjusted for the two stimulus types and 150 time points. To evaluate between-subject
258 consistency of the magnitudes of the largest deflections in the evoked responses in each
259 hemisphere and experiment, the average value over time points within ± 10 ms windows around
260 the peak latencies were calculated for each subject and submitted to *t*-tests with False discovery
261 rate (*fdr*) adjustment for 12 tests.

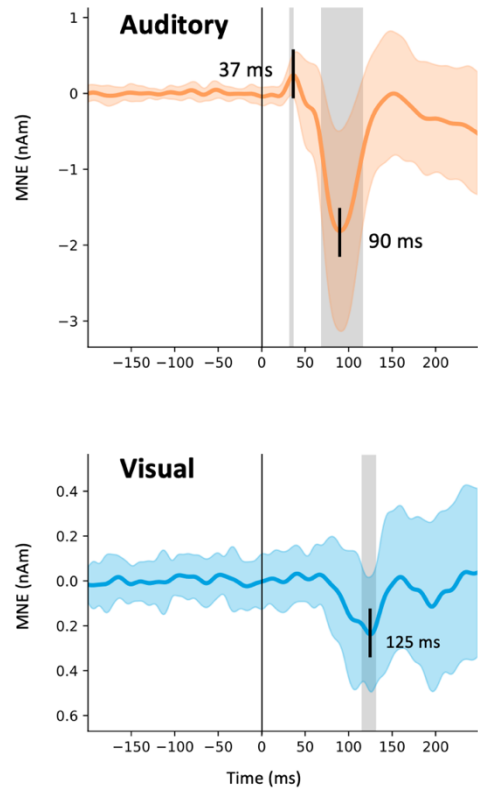
262 For the HNN models, a non-parametric resampling approach was used to test whether the
263 alternative models could provide a significantly better fit than our main models. First, the MEG
264 source waveforms for auditory and visual evoked responses were resampled by drawing from 32
265 signals (8 subjects x 2 hemispheres x 2 experiments) 500 times with replacement. The same was
266 repeated for 32 simulation runs for each of the models (FF + FB and FB). Next, the root-mean-
267 square error (RMSE) between each of the 500 resampled MEG signals and 500 resampled
268 simulations for each model was calculated, resulting in histograms of RMSE values within each
269 model. We tested whether the difference between the simulated source waveforms from the FB
270 vs. FF + FB models was significantly different from 0. The RMSE difference histograms were
271 normalized for each model between -1 and 1, as the ranges in the auditory and visual models
272 were different. To create a null-distribution, the signs of the waveforms were randomly flipped
273 10,000 times, an average of 500 resamplings was calculated. To assign a *p*-value for each model,
274 the mean RMSE value was compared with the null distribution, with the Bonferroni adjustment of
275 $n = 2$ (auditory and visual models). If the difference of the models (FF + FB vs. FB) was significant,
276 we concluded that including the first FF was necessary for the model.

277

278 **RESULTS**

279 ***MEG source waveforms in auditory cortex in response to auditory and visual stimuli***

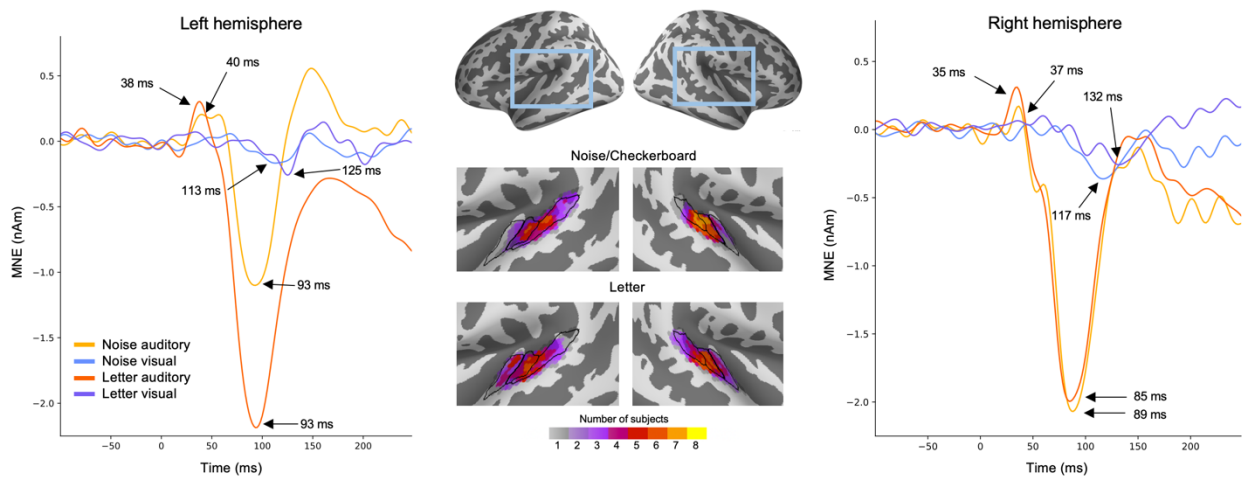
280 Estimated MEG source waveforms for auditory and visual evoked activity in the auditory cortex
281 ROIs, averaged over subjects, tasks, and hemispheres, are shown in **Fig. 2**. The auditory evoked
282 response showed a characteristic biphasic P50m-N100m waveform, with a positive peak at 37
283 and a negative peak at 90 ms after the onset of the auditory stimuli. These peak latencies are
284 similar to those reported previously for auditory noise burst stimuli (Hari et al., 1987). The cross-
285 sensory visual evoked response in the auditory cortex had a monophasic peak at 125 ms after
286 the appearance of the visual stimuli. The source magnitudes at the peak latencies were
287 significantly different from zero (t -test, $p < 0.05$, Bonferroni adjusted). The magnitude of the visual
288 evoked response was about 13% of the magnitude of the auditory N100m. The direction of the
289 source current for the visual response was the same as that of the auditory N100m response,
290 pointing from the gray matter towards the white matter.



291
292 **Figure 2.** MEG source activity in the auditory cortex. The estimated source waveforms in
293 response to the auditory (orange) and visual (blue) stimuli (mean and standard deviation across
294 subjects, hemispheres, and experiments). Negative values correspond to inward cortical currents,
295 i.e., pointing from the gray matter towards the white matter. The gray shading indicates time points
296 that differing significantly from zero (t -test, $p < 0.05$, Bonferroni adjusted).

297
298 We examined the reproducibility of the estimated source waveforms across the experiments,
299 hemispheres, and individual subjects. MEG source waveforms in the left and the right
300 hemispheres in response to the *Noise/Checkerboard* and *Letter* stimuli are illustrated in **Fig. 3**.
301 The magnitude of the auditory N100m was larger for the *Letter* than for the *Noise* stimuli in the
302 left hemisphere, but similar in the right hemisphere; this lateralization is expected for responses
303 to phonetic vs. non-verbal stimuli (Gootjes et al., 1999; Parviainen et al., 2005). The anatomical
304 overlap of ROIs across subjects (**Fig. 3**, middle panel) suggested that the prominent auditory

305 evoked responses originated mostly in the Heschl's sulcus and the anterior part of the planum
306 temporale. There were no clear differences in the location of the ROIs between the
307 *Noise/Checkerboard* and *Letter* experiments; however, for the *Letter* stimuli, the location
308 extended to the Heschl's gyrus in half of the subjects. The peak latencies of the auditory evoked
309 responses were similar within a few milliseconds in both experiments. For the visual evoked
310 response, a negative deflection with the peak latency ranging from 113 to 132 ms was seen in
311 both experiments in both hemispheres.

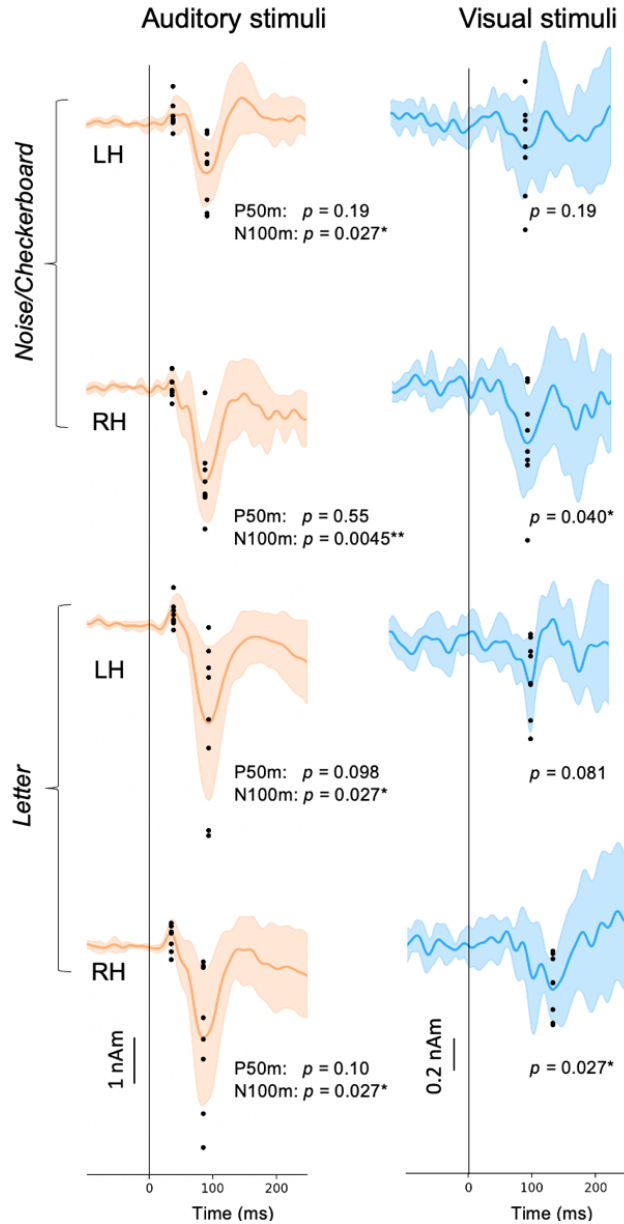


312
313 **Figure 3.** MEG source waveforms in the left and right hemisphere auditory cortex in response to
314 auditory and visual stimulation, shown separately for the *Noise/Checkerboard* and *Letter*
315 experiments. The source waveforms were averaged over subjects. The locations of the functional
316 ROIs morphed to common anatomical space ('fsaverage' from FreeSurfer) are shown in the
317 middle; the color bar indicates how many subjects' individual ROIs overlapped at each cortical
318 location. The black lines illustrate the Heschl's gyrus (anterior), Heschl's sulcus (middle) and part
319 of planum temporale (posterior).

320

321 To evaluate between-subject consistency of the largest deflections in the evoked responses in
322 each hemisphere in each experiment, we calculated for each subject the average value over time

323 points within ± 10 ms windows around the peak latencies (black dots in **Fig. 4**). The auditory
324 N100m peak was statistically significant in all cases (*Noise*: left hemisphere $p = 0.027$, right $p =$
325 0.0045 ; *Letter*: left $p = 0.027$, right $p = 0.027$; *t*-test, False discovery rate (*fdr*) adjusted). For the
326 response to the visual stimuli, the negative peak was statistically significant in the right
327 hemisphere (*Checkerboard*: $p = 0.040$; *Letter*: $p = 0.027$) but not in the left hemisphere
328 (*Checkerboard*: $p = 0.19$; *Letter*: $p = 0.$). The auditory P50m peaks were not significant when
329 calculated separately for the different cases, but they were significant for the grand average
330 responses (see **Fig. 2**).



331

332 **Figure 4.** Variation of the estimated source waveforms among individual subjects. The p-values

333 indicate the significance of the response magnitudes at the peak latencies (t-test; fdr adjusted).

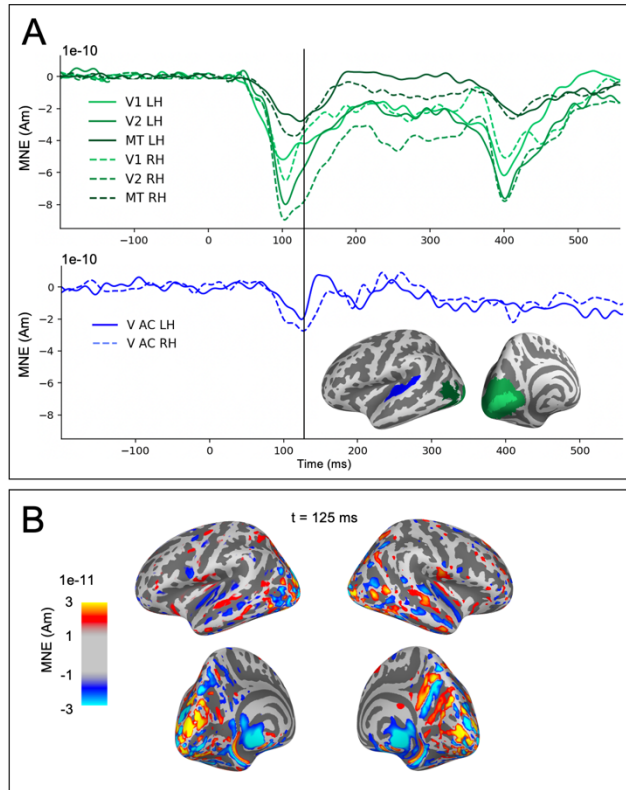
334 Continuous lines and shading: mean \pm standard deviation across subjects; black dots: response

335 magnitudes for individual subjects, calculated as the average over ± 10 ms time windows around

336 the peak latencies. LH: left hemisphere, RH: right hemisphere. * $p < 0.05$, ** $p < 0.01$.

337

338 The observed weak visual evoked activity in the auditory cortex partially coincided with strong
339 activity in occipital visual cortical regions (**Fig. 5**). The estimated auditory cortex source
340 waveforms could potentially reflect artefactual spread in the MEG source estimates due to activity
341 in other cortical regions responding to the visual stimuli. We examined this possibility in two ways.
342 First, we observed that the time course of the estimated sources for visual cortex ROIs had
343 prominent deflections for both the onset (with peak latencies at ~100 ms) and the offset (~400
344 ms) of the visual stimuli, whereas in the auditory cortex the response was seen mainly for the
345 onset only (**Fig. 5A**). If the onset and offset responses share a common spatial distribution in the
346 occipital cortex, then also the potential artefactual spreading to the auditory cortex is expected to
347 be the similar after the onset and the offset of the visual stimuli. However, this was not found in
348 the data. Second, the spatial maps of the source estimates for the visual evoked responses have
349 a gap between the weak auditory cortex activity and the large occipital cortex activity (**Fig. 5B**).
350 Artificial spread would be expected to be spatially uniform rather than forming separate foci in the
351 auditory cortex. These observations argue against the possibility of the cross-sensory visual
352 evoked response in the auditory cortex to be artefactually resulting from spread from visual cortex
353 in the source estimates.



354

355 **Figure 5.** Evaluation of potential artefactual spatial spread in the estimated MEG source activity
356 from visual cortex to the auditory ROIs. (A) Source time-courses (MNE, averaged across subjects
357 and tasks) in response to visual stimuli for occipital areas V1, V2, MT (green) and the auditory
358 cortices (V AC, blue). (B) Spatial maps of the MNE source estimate for the visual evoked activity
359 at the time of the largest peak in the response to visual stimuli in the auditory cortex.

360

361 **Neural modeling with HNN**

362 The initial manual tuning values for the mean (and standard deviation) of the time distribution
363 of the inputs were $\mu_{FF} = 35$ ($\sigma_{FF} = 3.0$) ms for the FF and $\mu_{FB} = 75$ ($\sigma_{FB} = 13.3$) ms for the FB
364 input in the auditory model, and $\mu_{FB} = 105$ ($\sigma_{FB} = 13.3$) ms for the FB input in the visual model.
365 The optimal scaling factor was found to be 53 for the auditory and 5 for the visual simulation. Fine-
366 tuning with Bayesian hyperparameter optimization resulted in only small adjustments to the timing
367 parameters. The optimized values were $\mu_{FF} = 34$ ($\sigma_{FF} = 1.0$), $\mu_{FB} = 74$ ($\sigma_{FB} = 14.0$) in the auditory

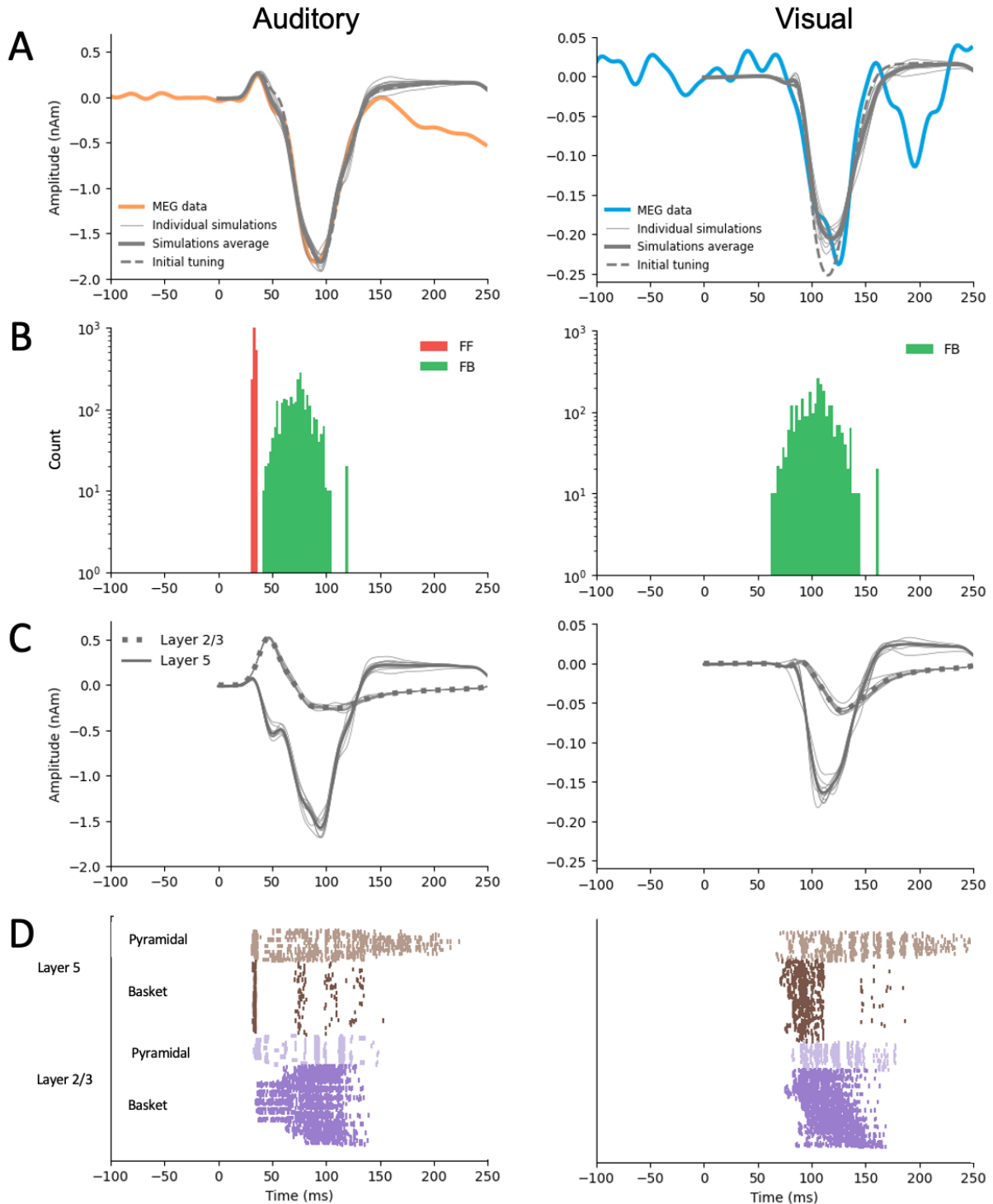
368 model, and $\mu_{FB} = 105$ ($\sigma_{FB} = 17.5$) in the visual model (**Table 1**). The temporal distributions of
 369 the inputs are depicted in **Fig. 6B**. For both the auditory responses (P50m-N100m) and the visual
 370 responses (peaking at 125 ms), the simulated source waveforms captured the main features of
 371 the experimentally observed MEG results (**Fig. 6A**).

372

373 **Table 1.** Comparison of HNN parameters for auditory and visual models. The mean μ and
 374 standard deviation σ (milliseconds) describe the temporal distribution of the inputs. Scaling factor
 375 is used to match the simulated dipole to the measured evoked response waveform. RMSE is root-
 376 mean-square error calculated between simulated and measured waveform. The main models are
 377 highlighted.

| Model | μ_{FF} (σ_{FF}) | μ_{FB} (σ_{FB}) | μ_{FF2} (σ_{FF2}) | Scaling | RMSE |
|--|------------------------------|------------------------------|--------------------------------|---------|-------|
| A: FF + FB + FF (Kohl et al., 2022) | 47 (3.0) | 81 (13.3) | 151 (11.1) | 1500 | |
| A: FF + FB + FF | 35 (1.0) | 77 (15.0) | 90 (14.4) | 57 | 0.15 |
| A: FF + FB | 34 (1.0) | 74 (14.0) | - | 53 | 0.072 |
| A: FB | - | 78 (14.8) | - | 38 | 0.23 |
| A: FF | 20 (3) | - | - | 1 | 0.86 |
| V: FF + FB | 42 (1.0) | 99 (12.7) | - | 6 | 0.012 |
| V: FB | - | 105 (17.5) | - | 5 | 0.024 |
| V: FF | 1 (3.0) | - | - | 1 | 0.095 |

378



379

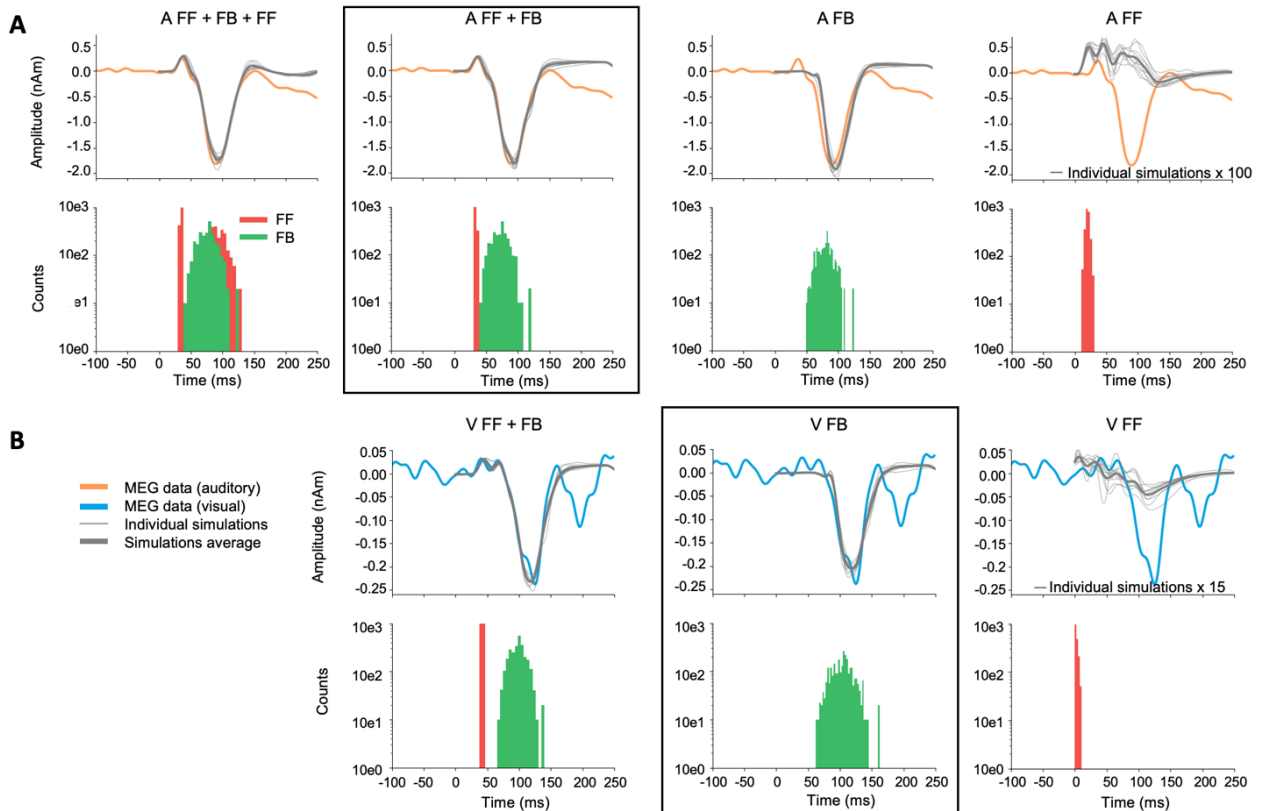
380 **Figure 6.** HNN simulations of the auditory cortex activity in response to auditory (left) and visual
381 (right) stimuli. **A:** Simulated source waveforms using the initial manual adjustments to the model
382 parameters (dashed gray lines), after parameter optimization (thick gray: average, thin gray: 10

383 *individual simulation runs), and the measured MEG data averaged over subjects, hemispheres,*
384 *and experiments (orange: auditory, blue: visual). **B**: Histograms of the timing of the inputs*
385 *sampled from a Gaussian distribution with a model-specific mean and standard deviation (red:*
386 *FF, green: FB) **C**: Layer-specific simulations after optimization (green: layer 2/3, purple: layer 5,*
387 *gray: 10 respective individual simulation runs). **D**: Spiking activity of the pyramidal and basket*
388 *cells in layers 2/3 and layer 5 (10 simulation runs).*

389

390 Further insights to the generation of the source currents can be obtained by plotting separately
391 the contributions from layer-2/3 and in layer-5 pyramidal cells (**Fig. 6C**) and the sequences of the
392 spiking activity of the four cell types included in the HNN model (**Fig. 6D**). In the model for the
393 auditory evoked response, FF input was assumed to arrive to the auditory cortex through the
394 middle cortical layer and the excite the basal dendrites of the pyramidal cells in both layers 2/3
395 and 5 (**Fig. 6C**, left). The net result of the FF input was an initial upward (positive) peak. The
396 arrival of the FB input to the distal parts of the apical dendrites of the pyramidal cells resulted in
397 reversal of the net current to be downwards. In the model for the cross-sensory visual evoked
398 response, the FB input arriving distally drove the net source current downwards within the apical
399 dendrites of both layer 2/3 and layer 5 pyramidal cells (**Fig. 6C**, right).

400 As HNN has a large number of parameters, it is possible that our chosen models are not the
401 only ones that can reproduce the experimentally observed MEG source waveforms. However,
402 HNN can serve us as a valuable hypothesis testing tool to test different models. Alternative
403 models with different combinations of FF and FB inputs are shown in **Fig. 7**, and the
404 corresponding optimized HNN parameters for these are listed in **Table 1**.



405

406 **Figure 7.** Alternative models for auditory (A) and visual (B) responses. The main models (A: FF
 407 + FB and V: FB) are framed. The experimentally observed MEG source waveforms (orange:
 408 auditory stimulus, blue: visual stimulus) are overlaid with the simulated waveforms (thin gray:
 409 10 individual simulation runs, thick gray: average of the individual runs). Histograms below the
 410 waveforms show the temporal distribution of FF (red) and FB (green) inputs to the HNN model of
 411 the auditory cortex neural circuit. FF only simulations are scaled to illustrate their waveforms
 412 compared with the MEG signal.

413

414 For the auditory evoked responses, inclusion of a later second FF input to the model had only
 415 little effect on the simulated source waveforms within 0–150 ms (A: FF+FB+FF2 vs. A: FF+FB,
 416 **Fig. 7A**). Removing the first FF input, however, resulted in a notable difference in the early time
 417 window (30–80 ms), during which the first upward deflection was seen in the MEG data.

418 Interestingly, if the FB input was removed, the FF input alone could not produce response
419 waveforms similar to those observed empirically. As the optimal scaling factor for the FF only
420 model was 1, **Fig. 7** (right column) shows the model scaled up in order to illustrate how the
421 waveform looks like compared with the MEG response. Thus, the FB input seems to have an
422 essential role in the generation of the evoked responses studied here.

423 For the visual evoked response, the difference between models with and without an FF input
424 (V: FF+FB vs. V: FB) was most pronounced in the early part (30–80 ms) of the simulated source
425 waveforms (**Fig. 7B**). However, although the V: FF+FB model slightly improved the fit to the
426 measured MEG signal in comparison with V: FB, considering the magnitude of the response with
427 the baseline noise level (see **Fig. 2**) suggests that the additional FF input in the model for the
428 response to the visual stimuli may be mostly explaining just noise in the data. Using a non-
429 parametric resampling approach, a significant difference between FF+FB vs. FB was found for
430 the auditory models ($p < 0.001$) but not for the visual models ($p = 0.39$). In other words, early FF
431 input did not significantly improve the model fit to the response to visual stimuli. Thus, these
432 results support our main hypothesis that the response to the auditory stimuli results from a
433 combination of FF and FB inputs to the auditory cortex, whereas the cross-sensory visual
434 response can be explained with just FB input to the auditory cortex.

435

436 **DISCUSSION**

437 The MEG data revealed a cross-sensory event-related response in the auditory cortex, peaking
438 at about 125 ms after the appearance of the visual stimuli. The direction of the estimated source
439 current for this response was the same as for the auditory N100m response, pointing from the
440 cortical gray matter towards the white matter. The main shape of the visual evoked response
441 waveform could be reproduced by an HNN model with FB-type input, whereas for the biphasic
442 P50m-N100m auditory evoked response both FF and FB inputs were needed. The experimental
443 and modeling results are consistent with the hypothesis that cross-sensory visual input to the
444 auditory cortex is of FB type (Schroeder and Foxe, 2002).

445 ***Characterization of cross-sensory visual evoked activation in auditory cortex***

446 Recently, Kohl et al. presented an HNN model with a sequence of FF and FB inputs explaining
447 several properties of auditory evoked responses in the auditory cortex (Kohl et al., 2022). With
448 only minor adjustments to the input timings and the overall scaling, the model could be adapted
449 to explain the MEG source waveforms for the auditory evoked responses observed in the present
450 study. A sequence of FF-FB (and -FF) inputs has been shown to model well also somatosensory
451 responses in the somatosensory cortex (Jones et al., 2007). In contrast, to explain the early part
452 of the cross-sensory visual response in the auditory cortex, we found that a model with only an
453 FB input, without a preceding FF input, was adequate. The FB-type characteristics is consistent
454 with previous NHP electrophysiological studies (Schroeder and Foxe, 2002). Multi-contact
455 electrode recordings in the macaque have shown early activity in the granular (middle) layer of
456 auditory cortex in response to auditory stimuli, suggesting FF-type input, whereas cross-sensory
457 visual evoked activity appeared first in supra- and infragranular layers (Schroeder and Foxe,
458 2002). Similar laminar properties in the auditory cortex have also been seen in human fMRI
459 studies (Gau et al., 2020; Chai et al., 2021; Lankinen et al., 2022). In the high-field laminar fMRI
460 study of Lankinen et al. (2022), which used the same stimuli as in the *Noise/Checkerboard*

461 experiment in the present MEG study, BOLD signal depth profiles in the auditory cortex showed
462 different curvature for auditory vs. visual stimuli, consistent with the hypothesized difference in
463 the FF vs. FB type inputs.

464 There are several possible neural pathways for the visual evoked activity to reach the auditory
465 cortex. The relatively long latency of the visual response observed here is consistent with what
466 would be expected from input from higher-order polysensory areas such as the superior temporal
467 sulcus (Foxe and Schroeder, 2005). However, the present analyses focusing on activity within
468 auditory cortex only do not reveal the origin of the inputs to the auditory cortex. That type of
469 information could be deduced, e.g., from Granger-causality measures between estimated source
470 waveforms in multiple cortical areas (Milde et al., 2011; Gow and Nied, 2014; Michalareas et al.,
471 2016).

472 Interestingly, NHP studies have shown different characteristics for visual and somatosensory
473 cross-sensory inputs to the auditory cortex: FB-type for visual but FF-type for somatosensory
474 (Schroeder and Foxe, 2002). The role of different types of cross-sensory inputs to the auditory
475 cortex may have important implications to theories of multisensory processing (Schroeder and
476 Foxe, 2005). There appear to be multiple ways how cross-sensory processes may be influenced
477 by the hierarchical organization among brain areas. FB-type inputs are commonly associated with
478 modulatory influences, whereas FF-type inputs are more directly related to sensory information
479 (Schroeder and Foxe, 2005).

480 ***Complementary approaches to noninvasive detection of FF and FB processes***

481 The present approach of combining MEG and cellular-level computational modeling complements
482 other non-invasive methods for studying the organization of cortical processes in the human brain.
483 The millisecond-scale time resolution of MEG and EEG enables the investigation of fast dynamics
484 of the brain activity, which is not attainable with hemodynamic fMRI. High-field fMRI, however,
485 can provide laminar-level spatial resolution for making inferences about FF and FB activity (see

486 e.g., De Martino et al., 2018; Lawrence et al., 2019b; Norris and Polimeni, 2019). With certain
487 strong assumptions about the location and extent of the spatial distribution, layer-specific source
488 localization in MEG has also been demonstrated (Bonaiuto et al., 2018a; Bonaiuto et al., 2018b).
489 FF/FB influences can also be inferred from directed connectivity measures for MEG source
490 estimates at specific frequency bands (Michalareas et al., 2016).

491 The present results also support the view that the direction of MEG source waveforms can be
492 useful for inferring information about the hierarchical organization of cortical processing (Ahlfors
493 et al., 2015). In particular, FF-type input to the supragranular layer, with excitatory synaptic
494 connections to the distal part of the apical dendrites of pyramidal cells, is likely to be a major
495 contributor to the downward-directed MEG source currents (Lopes da Silva, 2010; Ahlfors and
496 Wreh, 2015). There was a general correspondence between the source direction and the type of
497 input in the HNN model: the outward directed source current during the auditory P50m response
498 was associated with FF input in HNN, whereas FB inputs were needed to model the inward source
499 currents during the auditory N100m and the visual response peaking at 125 ms. A close
500 relationship between the direction of MEG source currents and FF- vs. FB-type inputs has also
501 been found in HNN modeling of somatosensory response in the primary somatosensory cortex
502 (Jones et al., 2007). Furthermore, the direction of the MEG source currents in inferior
503 occipitotemporal cortex has been found to reverse between two experimental conditions for which
504 a cognitive neuroscience theory for visual object recognition predicted FF vs. FB inputs to the
505 area (Ahlfors et al., 2015).

506 ***Limitations of the current study***

507 Localizing weak cross-sensory visual evoked activity in the auditory cortex is challenging because
508 of potential interference in the MEG source estimate from the partially coinciding occipital cortex
509 activity. However, both the shape of the time courses and the patterns in the spatial distributions
510 of the source estimates (see **Fig. 6**) suggested that it was unlikely that the visual evoked activity

511 in the auditory cortex was due to artefactual long-range crosstalk caused by spatial spread in the
512 source estimates. Short-range spread in the source estimates can also confound the
513 interpretation of the source waveforms. If the true location of the visual responses were not within
514 the auditory cortex ROI, but, e.g., in the opposite side of the superior temporal gyrus, the source
515 direction could become incorrectly identified. Combining MEG with high-resolution fMRI could
516 help to confirm the location of the activity. It is also possible that there was simultaneous activity
517 in multiple auditory areas in the supratemporal plane. Most of the individual subjects' ROIs were
518 located directly at the primary auditory regions, at or near the at Heschl's sulcus, being thus
519 slightly different than the auditory association area just posterior to primary auditory region studied
520 by Schroeder and Foxe (2002). However, it has been shown in monkeys that such FF type
521 patterns are typical throughout the core and belt regions of auditory cortex (Schroeder et al. 2001).
522 Without further data, e.g., intracranial recordings, it is difficult to conclusively resolve the locations
523 of the sources of the observed cross-sensory MEG response.

524 HNN, and biophysical computational neural modeling in general, has two challenges of
525 opposite nature: the neural circuit model is complex, with a large number of adjustable
526 parameters, and yet the model is a simplified representation of the cortical circuitry. We used
527 neural circuit parameters of the pre-tuned model for auditory evoked responses in the auditory
528 cortex by Kohl et al. (2022) and only adjusted a small number of selected parameters, focusing
529 on the timing of the FF and FB inputs. Given the limited SNR of the experimental source
530 waveforms, we did not attempt to vary the neural connectivity parameters. We cannot exclude
531 the possibility that there could be some combinations within the high-dimensional parameter
532 space that could explain the responses with a very different circuit model than the one reported
533 here. Useful in future studies, it has been recently demonstrated that combining simulation-based
534 inference (SBI) to HNN modeling can help in parameter estimation (Tolley et al., 2023).

535 We modeled only one local region (auditory cortex) receiving one-directional external inputs.
536 To determine where the inputs are arriving from and where the information will be sent, directional
537 connectivity analyses between multiple regions would be needed. Thus, further studies would be
538 necessary to connect other areas of interest to the network. Furthermore, combining MEG with
539 layer-specific fMRI could provide complementary information which could help to build a more
540 detailed picture of the FF/FB influences.

541 ***Conclusions***

542 The combined MEG and HNN modeling results support the hypothesis that cross-sensory visual
543 input to the auditory cortex is of FB type. The results also illustrate how the dynamic patterns of
544 the estimated MEG/EEG source activity can provide information about the characteristics of the
545 input into the cortical areas in terms of hierarchical organization among the cortical areas.
546 Avenues for future research could include connecting other areas of interest to the network,
547 calculating directed (effective) connectivity measures between cortical areas specifically, and
548 combining complementary information from MEG data with layer-specific fMRI to build a more
549 detailed picture of the FF/FB influences.

550

551 **References**

- 552 Ahlfors SP, Wreh C, 2nd (2015) Modeling the effect of dendritic input location on MEG and EEG
553 source dipoles. *Med Biol Eng Comput* 53:879-887.
- 554 Ahlfors SP, Jones SR, Ahveninen J, Hämäläinen MS, Belliveau JW, Bar M (2015) Direction of
555 magnetoencephalography sources associated with feedback and feedforward
556 contributions in a visual object recognition task. *Neurosci Lett* 585:149-154.
- 557 Ahveninen J, Chang WT, Huang S, Keil B, Kopco N, Rossi S, Bonmassar G, Witzel T, Polimeni
558 JR (2016) Intracortical depth analyses of frequency-sensitive regions of human auditory
559 cortex using 7TfMRI. *Neuroimage* 143:116-127.
- 560 Aine CJ, Stephen JM, Christner R, Hudson D, Best E (2003) Task relevance enhances early
561 transient and late slow-wave activity of distributed cortical sources. *J Comput Neurosci*
562 15:203-221.
- 563 Allison T, Puce A, McCarthy G (2002) Category-sensitive excitatory and inhibitory processes in
564 human extrastriate cortex. *J Neurophysiol* 88:2864-2868.
- 565 Bonaiuto JJ, Little S, Neymotin SA, Jones SR, Barnes GR, Bestmann S (2021) Laminar dynamics
566 of high amplitude beta bursts in human motor cortex. *Neuroimage* 242:118479.
- 567 Bonaiuto JJ, Meyer SS, Little S, Rossiter H, Callaghan MF, Dick F, Barnes GR, Bestmann S
568 (2018a) Lamina-specific cortical dynamics in human visual and sensorimotor cortices.
569 *Elife* 7.
- 570 Bonaiuto JJ, Rossiter HE, Meyer SS, Adams N, Little S, Callaghan MF, Dick F, Bestmann S,
571 Barnes GR (2018b) Non-invasive laminar inference with MEG: Comparison of methods
572 and source inversion algorithms. *Neuroimage* 167:372-383.
- 573 Cauller LJ, Kulics AT (1991) The neural basis of the behaviorally relevant N1 component of the
574 somatosensory-evoked potential in SI cortex of awake monkeys: evidence that backward
575 cortical projections signal conscious touch sensation. *Exp Brain Res* 84:607-619.

576 Chai Y, Liu TT, Marrett S, Li L, Khojandi A, Handwerker DA, Alink A, Muckli L, Bandettini PA
577 (2021) Topographical and laminar distribution of audiovisual processing within human
578 planum temporale. *Prog Neurobiol* 205:102121.

579 Dale AM, Liu AK, Fischl BR, Buckner RL, Belliveau JW, Lewine JD, Halgren E (2000) Dynamic
580 statistical parametric mapping: combining fMRI and MEG for high-resolution imaging of
581 cortical activity. *Neuron* 26:55-67.

582 De Martino F, Moerel M, Xu J, van de Moortele PF, Ugurbil K, Goebel R, Yacoub E, Formisano
583 E (2015) High-Resolution Mapping of Myeloarchitecture In Vivo: Localization of Auditory
584 Areas in the Human Brain. *Cereb Cortex* 25:3394-3405.

585 De Martino F, Yacoub E, Kemper V, Moerel M, Uludag K, De Weerd P, Ugurbil K, Goebel R,
586 Formisano E (2018) The impact of ultra-high field MRI on cognitive and computational
587 neuroimaging. *Neuroimage* 168:366-382.

588 Destrieux C, Fischl B, Dale A, Halgren E (2010) Automatic parcellation of human cortical gyri and
589 sulci using standard anatomical nomenclature. *Neuroimage* 53:1-15.

590 Felleman DJ, Van Essen DC (1991) Distributed hierarchical processing in the primate cerebral
591 cortex. *Cereb Cortex* 1:1-47.

592 Finn ES, Huber L, Jangraw DC, Molfese PJ, Bandettini PA (2019) Layer-dependent activity in
593 human prefrontal cortex during working memory. *Nat Neurosci* 22:1687-1695.

594 Fischl B (2012) FreeSurfer. *Neuroimage* 62:774-781.

595 Fischl B, Rajendran N, Busa E, Augustinack J, Hinds O, Yeo BT, Mohlberg H, Amunts K, Zilles K
596 (2008) Cortical folding patterns and predicting cytoarchitecture. *Cereb Cortex* 18:1973-
597 1980.

598 Fischl B, van der Kouwe A, Destrieux C, Halgren E, Segonne F, Salat DH, Busa E, Seidman LJ,
599 Goldstein J, Kennedy D, Caviness V, Makris N, Rosen B, Dale AM (2004) Automatically
600 parcellating the human cerebral cortex. *Cereb Cortex* 14:11-22.

- 601 Foxe J, Morocz I, Murray M, Higgins B, Javitt D, Schroeder C (2000) Multisensory auditory-
602 somatosensory interactions in early cortical processing revealed by high-density electrical
603 mapping. *Cognitive Brain Research* 10:77-83.
- 604 Foxe JJ, Schroeder CE (2005) The case for feedforward multisensory convergence during early
605 cortical processing. *Neuroreport* 16:419-423.
- 606 Fracasso A, Luijten PR, Dumoulin SO, Petridou N (2018) Laminar imaging of positive and
607 negative BOLD in human visual cortex at 7T. *Neuroimage* 164:100-111.
- 608 Gau R, Bazin PL, Trampel R, Turner R, Noppeney U (2020) Resolving multisensory and
609 attentional influences across cortical depth in sensory cortices. *Elife* 9.
- 610 Ghazanfar AA, Schroeder CE (2006) Is neocortex essentially multisensory? *Trends Cogn Sci*
611 10:278-285.
- 612 Giard M, Peronnet F (1999) Auditory-visual integration during multimodal object recognition in
613 humans: a behavioral and electrophysiological study. *Journal of Cognitive Neuroscience*
614 11:473-490.
- 615 Gootjes L, Raij T, Salmelin R, Hari R (1999) Left-hemisphere dominance for processing of vowels:
616 a whole-scalp neuromagnetic study. *Neuroreport* 10:2987-2991.
- 617 Gow DW, Jr., Nied AC (2014) Rules from words: a dynamic neural basis for a lawful linguistic
618 process. *PLoS One* 9:e86212.
- 619 Gramfort A, Luessi M, Larson E, Engemann DA, Strohmeier D, Brodbeck C, Parkkonen L,
620 Hamalainen MS (2014) MNE software for processing MEG and EEG data. *Neuroimage*
621 86:446-460.
- 622 Gramfort A, Luessi M, Larson E, Engemann DA, Strohmeier D, Brodbeck C, Goj R, Jas M, Brooks
623 T, Parkkonen L, Hamalainen M (2013) MEG and EEG data analysis with MNE-Python.
624 *Front Neurosci* 7:267.

- 625 Hämäläinen M, Hari R, Ilmoniemi R, Knuutila J, Lounasmaa O (1993) Magnetoencephalography
626 -theory, instrumentation, and applications to noninvasive studies of the working human
627 brain. *Rev Mod Phys* 65:413-497.
- 628 Hamalainen MS, Ilmoniemi RJ (1994) Interpreting magnetic fields of the brain: minimum norm
629 estimates. *Med Biol Eng Comput* 32:35-42.
- 630 Hari R, Aittoniemi K, Jarvinen ML, Katila T, Varpula T (1980) Auditory evoked transient and
631 sustained magnetic fields of the human brain. Localization of neural generators. *Exp Brain*
632 *Res* 40:237-240.
- 633 Hari R, Pelizzone M, Makela JP, Hallstrom J, Leinonen L, Lounasmaa OV (1987) Neuromagnetic
634 responses of the human auditory cortex to on- and offsets of noise bursts. *Audiology*
635 26:31-43.
- 636 Head TK, Manor; Nahrstaedt, Holger; Louppe, Gilles; Shcherbatyi, Iaroslav; (2020) scikit-
637 optimize. In.
- 638 Inui K, Kakigi R (2006) Temporal analysis of the flow from V1 to the extrastriate cortex in humans.
639 *J Neurophysiol* 96:775-784.
- 640 Inui K, Wang X, Tamura Y, Kaneoke Y, Kakigi R (2004) Serial processing in the human
641 somatosensory system. *Cereb Cortex* 14:851-857.
- 642 Inui K, Okamoto H, Miki K, Gunji A, Kakigi R (2006) Serial and parallel processing in the human
643 auditory cortex: a magnetoencephalographic study. *Cereb Cortex* 16:18-30.
- 644 Jones SR, Pritchett DL, Stufflebeam SM, Hamalainen M, Moore CI (2007) Neural correlates of
645 tactile detection: a combined magnetoencephalography and biophysically based
646 computational modeling study. *J Neurosci* 27:10751-10764.
- 647 Jones SR, Pritchett DL, Sikora MA, Stufflebeam SM, Hamalainen M, Moore CI (2009) Quantitative
648 analysis and biophysically realistic neural modeling of the MEG mu rhythm:
649 rhythmogenesis and modulation of sensory-evoked responses. *J Neurophysiol* 102:3554-
650 3572.

- 651 Kayser C, Logothetis NK (2007) Do early sensory cortices integrate cross-modal information?
652 Brain Struct Funct 212:121-132.
- 653 Khan S, Michmizos K, Tommerdahl M, Ganesan S, Kitzbichler MG, Zetino M, Garel KL, Herbert
654 MR, Hamalainen MS, Kenet T (2015) Somatosensory cortex functional connectivity
655 abnormalities in autism show opposite trends, depending on direction and spatial scale.
656 Brain 138:1394-1409.
- 657 Klein BP, Fracasso A, van Dijk JA, Paffen CLE, Te Pas SF, Dumoulin SO (2018) Cortical depth
658 dependent population receptive field attraction by spatial attention in human V1.
659 Neuroimage 176:301-312.
- 660 Kohl C, Parviainen T, Jones SR (2022) Neural Mechanisms Underlying Human Auditory Evoked
661 Responses Revealed By Human Neocortical Neurosolver. Brain Topogr 35:19-35.
- 662 Kok P, Bains LJ, van Mourik T, Norris DG, de Lange FP (2016) Selective Activation of the Deep
663 Layers of the Human Primary Visual Cortex by Top-Down Feedback. Curr Biol 26:371-
664 376.
- 665 Lakatos P, Chen CM, O'Connell MN, Mills A, Schroeder CE (2007) Neuronal oscillations and
666 multisensory interaction in primary auditory cortex. Neuron 53:279-292.
- 667 Lankinen K, Ahlfors SP, Mamashli F, Blazejewska AI, Raij T, Turpin T, Polimeni JR, Ahveninen J
668 (2022) Cortical depth profiles of auditory and visual 7 T functional MRI responses in human
669 superior temporal areas. Hum Brain Mapp.
- 670 Law RG, Pugliese S, Shin H, Sliva DD, Lee S, Neymotin S, Moore C, Jones SR (2022)
671 Thalamocortical Mechanisms Regulating the Relationship between Transient Beta Events
672 and Human Tactile Perception. Cereb Cortex 32:668-688.
- 673 Lawrence SJ, Norris DG, de Lange FP (2019a) Dissociable laminar profiles of concurrent bottom-
674 up and top-down modulation in the human visual cortex. Elife 8.
- 675 Lawrence SJD, Formisano E, Muckli L, de Lange FP (2019b) Laminar fMRI: Applications for
676 cognitive neuroscience. Neuroimage 197:785-791.

- 677 Lee S, Jones SR (2013) Distinguishing mechanisms of gamma frequency oscillations in human
678 current source signals using a computational model of a laminar neocortical network. *Front*
679 *Hum Neurosci* 7:869.
- 680 Linden H, Pettersen KH, Einevoll GT (2010) Intrinsic dendritic filtering gives low-pass power
681 spectra of local field potentials. *J Comput Neurosci* 29:423-444.
- 682 Lopes da Silva FH (2010) Electrophysiological basis of MEG signals. In: *MEG: An introduction to*
683 *methods* (Hansen PC, Kringelbach, M.L., Salmelin, R., ed), pp 1-23. New York, New York:
684 Oxford University Press.
- 685 Michalareas G, Vezoli J, van Pelt S, Schoffelen JM, Kennedy H, Fries P (2016) Alpha-Beta and
686 Gamma Rhythms Subserve Feedback and Feedforward Influences among Human Visual
687 Cortical Areas. *Neuron* 89:384-397.
- 688 Milde T, Putsche P, Schwab K, Wacker M, Eiselt M, Witte H (2011) Dynamics of directed
689 interactions between brain regions during interburst-burst EEG patterns in quiet sleep of
690 full-term neonates. *Neurosci Lett* 488:148-153.
- 691 Moerel M, De Martino F, Ugurbil K, Formisano E, Yacoub E (2018) Evaluating the Columnar
692 Stability of Acoustic Processing in the Human Auditory Cortex. *J Neurosci* 38:7822-7832.
- 693 Moerel M, De Martino F, Ugurbil K, Yacoub E, Formisano E (2019) Processing complexity
694 increases in superficial layers of human primary auditory cortex. *Sci Rep* 9:5502.
- 695 Molholm S, Ritter W, Javitt DC, Foxe JJ (2004) Multisensory visual-auditory object recognition in
696 humans: a high-density electrical mapping study. *Cereb Cortex* 14:452-465.
- 697 Molholm S, Ritter W, Murray M, Javitt D, Schroeder C, Foxe J (2002) Multisensory auditory-visual
698 interactions during early sensory processing in humans: a high-density electrical mapping
699 study. *Cognitive Brain Research* 14:115-128.
- 700 Muckli L, De Martino F, Vizioli L, Petro LS, Smith FW, Ugurbil K, Goebel R, Yacoub E (2015)
701 Contextual Feedback to Superficial Layers of V1. *Curr Biol* 25:2690-2695.

- 702 Neymotin SA, Daniels DS, Caldwell B, McDougal RA, Carnevale NT, Jas M, Moore CI, Hines ML,
703 Hamalainen M, Jones SR (2020) Human Neocortical Neurosolver (HNN), a new software
704 tool for interpreting the cellular and network origin of human MEG/EEG data. *Elife* 9.
705 Norris DG, Polimeni JR (2019) Laminar (f)MRI: A short history and future prospects. *Neuroimage*
706 197:643-649.
- 707 Okada YC, Wu J, Kyuhou S (1997) Genesis of MEG signals in a mammalian CNS structure.
708 *Electroencephalogr Clin Neurophysiol* 103:474-485.
- 709 Parviainen T, Helenius P, Salmelin R (2005) Cortical differentiation of speech and nonspeech
710 sounds at 100 ms: implications for dyslexia. *Cereb Cortex* 15:1054-1063.
- 711 Picton TW, Hillyard SA, Krausz HI, Galambos R (1974) Human auditory evoked potentials. I.
712 Evaluation of components. *Electroencephalogr Clin Neurophysiol* 36:179-190.
- 713 Pinotsis DA, Geerts JP, Pinto L, FitzGerald THB, Litvak V, Aukstulewicz R, Friston KJ (2017)
714 Linking canonical microcircuits and neuronal activity: Dynamic causal modelling of laminar
715 recordings. *Neuroimage* 146:355-366.
- 716 Polimeni JR, Fischl B, Greve DN, Wald LL (2010) Laminar analysis of 7T BOLD using an imposed
717 spatial activation pattern in human V1. *Neuroimage* 52:1334-1346.
- 718 Raij T, Ahveninen J, Lin FH, Witzel T, Jaaskelainen IP, Letham B, Israeli E, Sahyoun C, Vasios
719 C, Stufflebeam S, Hamalainen M, Belliveau JW (2010) Onset timing of cross-sensory
720 activations and multisensory interactions in auditory and visual sensory cortices. *Eur J*
721 *Neurosci* 31:1772-1782.
- 722 Rockland KS, Pandya DN (1979) Laminar origins and terminations of cortical connections of the
723 occipital lobe in the rhesus monkey. *Brain Res* 179:3-20.
- 724 Schroeder CE, Foxe JJ (2002) The timing and laminar profile of converging inputs to multisensory
725 areas of the macaque neocortex. *Brain Res Cogn Brain Res* 14:187-198.
- 726 Schroeder CE, Foxe J (2005) Multisensory contributions to low-level, 'unisensory' processing.
727 *Curr Opin Neurobiol* 15:454-458.

- 728 Sherman MA, Lee S, Law R, Haegens S, Thorn CA, Hamalainen MS, Moore CI, Jones SR (2016)
729 Neural mechanisms of transient neocortical beta rhythms: Converging evidence from
730 humans, computational modeling, monkeys, and mice. *Proc Natl Acad Sci U S A*
731 113:E4885-4894.
- 732 Sliva DD, Black CJ, Bowary P, Agrawal U, Santoyo JF, Philip NS, Greenberg BD, Moore CI,
733 Jones SR (2018) A Prospective Study of the Impact of Transcranial Alternating Current
734 Stimulation on EEG Correlates of Somatosensory Perception. *Front Psychol* 9:2117.
- 735 Talsma D, Doty TJ, Woldorff MG (2007) Selective attention and audiovisual integration: is
736 attending to both modalities a prerequisite for early integration? *Cereb Cortex* 17:679-690.
- 737 Teder-Sälejärvi W, McDonald J, Di Russo F, Hillyard S (2002) An analysis of audio-visual
738 crossmodal integration by means of event-related potential (ERP) recordings. *Cognitive*
739 *Brain Research* 14:106-114.
- 740 Tolley N, Rodrigues PLC, Gramfort A, Jones S (2023) Methods and considerations for estimating
741 parameters in biophysically detailed neural models with simulation based inference.
742 *bioRxiv*.
- 743 Uutela K, Taulu S, Hamalainen M (2001) Detecting and correcting for head movements in
744 neuromagnetic measurements. *Neuroimage* 14:1424-1431.
- 745 Wu PY, Chu YH, Lin JL, Kuo WJ, Lin FH (2018) Feature-dependent intrinsic functional
746 connectivity across cortical depths in the human auditory cortex. *Sci Rep* 8:13287.
- 747 Zeki S (2018) The Rough Seas of Cortical Cartography. *Trends Neurosci* 41:242-244.
- 748 Ziegler DA, Pritchett DL, Hosseini-Varnamkhasi P, Corkin S, Hamalainen M, Moore CI, Jones
749 SR (2010) Transformations in oscillatory activity and evoked responses in primary
750 somatosensory cortex in middle age: a combined computational neural modeling and
751 MEG study. *Neuroimage* 52:897-912.
- 752